International Journal of Fluid Dynamics (1998), Vol. 2, Article 1

Simulated Flow around Long Rectangular Plates under Cross Flow Perturbations

B.T. Tan, M.C. Thompson, K. Hourigan

Fluid-dynamics Laboratory for Aeronautical and Industrial Research (FLAIR)
Department of Mechanical Engineering,
Monash University, Clayton, Victoria, Australia
(First received 5th June 1998; and in revised form 30th November 1998.
Published 22nd December 1998.)

Abstract

Numerical simulations of flow past long rectangular plates of various aspect ratios are performed. Comparisons are made with previous experimental and computational results. Simulations without external forcing show the stepwise increase in Strouhal number based on chord length characteristic of the *Impinging Shear Layer Instability*; in the present case, the shear layer develops into shed vortices upstream of the impingement for longer plates. Simulations with a small amplitude crossflow oscillatory forcing also exhibit a similar receptivity at these Strouhal numbers. This is demonstrated by Strouhal number stepping corresponding to local maxima of base suction as the plate aspect ratio is varied. Flow visualisations and animations indicate that the stepping corresponds to a similar integer mode of shedding as observed in the unperturbed case and reveals the phase relationship between leading- and trailing-edge shedding.

Keywords: Rectangular Plates, Perturbed Flow, Vortex Shedding, Base Pressure, Acoustic Forcing

Copyright This material is the work of the authors listed here. It is original and has not been published previously unless acknowledged. It may be freely copied and distributed provided that the names of the authors, the institutions and the journal remain attached.

1. Introduction

Bluff body flow dynamics is an area of fluid mechanics which underpins important engineering applications such as structural loading and design, aerodynamic drag reduction, and improving heat transfer devices. Much research has been devoted to flow around short bodies such as circular cylinders and normal flat plates (*e.g.*, Bearman and Trueman, 1972; Bearman, 1984; Bearman and Obasaju, 1982; Roshko, 1961; Williamson, 1988). In this article, the flow past elongated rectangular plates is addressed. Whilst for symmetrical short bodies, there is predominantly a single shear layer separating from the top and bottom leading edges, longer bodies introduce the additional complexity of allowing strong shear layer separation from both the leading and trailing edges. The interaction between the resultant vortex structures will be shown to lead to interesting and unexpected flow dynamics.

The basic flow considered in this article is shown in the diagram below. A two-dimensional long rectangular plate is placed in a uniform background flow. Shear layers separate from the leading edges of the plate and shed vortices which are convected downstream. At the trailing edge the shear layers may or may not roll up into vortices depending on system parameters. For the perturbed cases an external crossflow sinusoidal forcing is applied.

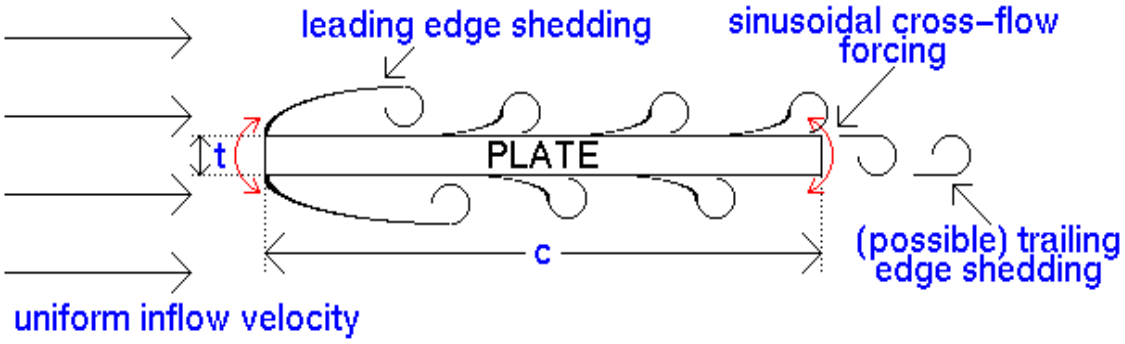


Figure 1: Schematic showing parameters involved and idealised vortical structures from the leading and trailing edges.

Once the leading-edge shedding is well established (for Reynolds numbers in excess of about 300), for plates longer than approximately 8 plate widths (t), the shear layer separating from the leading edge always reattaches to the long surface of the plate leading to discrete vortices passing the trailing edge. Nakamura *et al.* (1991) demonstrate this through visualisations at Re=1000. With the application of external forcing, it is possible to influence the vortex shedding from the leading edge over a narrow frequency range (Stokes and Welsh, 1986 ; Soria and Wu, 1992). On the other hand, trailing-edge shedding from bluff bodies is controlled locally by an absolute instability (Koch, 1985) and it is therefore difficult to shift the shedding frequency significantly; a graphic example of trailing-edge vortex shedding locking on to an acoustic resonance is shown in the animation provided in the review article by Parker (1997).

At low Reynolds numbers (Re = 1,000), Nakamura *et al.* (1991) observed that the Strouhal number based on plate chord increases in a step-wise manner for chord-to-thickness (c/t) ratios of 3-15; this was concluded to be a result of the *impinging shear layer instability* (Rockwell and Naudascher, 1979). It was conjectured by Nakamura *et al.* (1991) that for aspect ratios in the range $3.2 < c/t < 7.6$, the flapping of the leading-edge shear layer interacts directly with the trailing edge of the plate. This leads to the emission of a pressure pulse which controls the evolution of the leading-edge shear layer after a transition period when the feedback loop is established. Mills *et al.* (1995) observed that for plates longer than approximately c/t = 8, the shear layer does not directly interact with the trailing edge but rolls up and sheds vortices which in turn travel downstream and interact with the trailing edge. Again, this is hypothesised to result in pressure waves that travel upstream to lock the leading-edge shedding. This *vorticity impingment instability* is proposed to be generalisation of the impinging shear layer instability which includes impingment in the form of vortices as well as shear layers. If the convection speed of vortices along the plate is approximately constant, this causes the shedding frequency to vary inversely with plate chord (or length), so that the Strouhal number based on chord remains approximately constant. In addition, it is not necessary for the trailing to leading-edge pressure pulse to control the next shed vortex; it can control the second, third or fourth subsequently shed vortex, depending on plate length. Thus, each Strouhal number step corresponds to a different integer number of vortices (n) distributed along the plate.

Several numerical simulations have also modelled this behaviour. Okajima *et al.* (1990) simulated the flow for Reynolds numbers in the range [100,1200] and aspect ratios c/t between 0.4 and 8. They showed the abrupt change in shedding frequency at specific aspect ratios except for Re=250 and below. Okajima *et al.* (1992), Ozono *et al.* (1992) and Ohya *et al.* (1992) demonstrated the same stepping at Re = 1,000 for c/t = 3-9. For longer plates, the feedback was not strong enough to lock the leading-edge shedding and no single frequency dominated. Nakayama *et al.* (1993) performed simulations at Re = 200 and 400 and for c/t = 3-10. At Re = 200, the shedding frequency was approximately constant because there was no shedding from the leading edge but at Re = 400 the same stepping was observed for all plate lengths studied.

Except for very short plates (with c/t approximately 3), at high Reynolds numbers (*e.g.*, Stokes and Welsh, 1986 (Re = 15,000-30,000); Mills *et al.*, 1995 (Re = 9,000); Nakamura *et al.*, 1991 (Re > 2000)), the impinging shear layer instability does not appear to be sufficiently strong to lock the leading-edge shedding

and lead to the Strouhal number stepping. However, if the flow is perturbed externally, either directly or indirectly, the same receptivity is still apparent. There are at least two important cases here. The first was demonstrated by Stokes and Welsh (1986) who enclosed the plate in a duct. As the leading-edge vortices pass the trailing edge, acoustic energy can be fed into or removed from the natural resonant acoustic field of the duct. If the frequency at which vortices pass the trailing edge matches the resonant frequency, then the resonant field can build up and in turn control the leading-edge shedding. Thus an indirect feedback loop can be developed. In these experiments the flow velocity rather than plate chord was used as the control parameter. They observed peaks in the duct acoustic resonance amplitude which corresponded to locked shedding as the flow velocity was increased. By plotting the Strouhal numbers (based on chord) for which the shedding is locked to the acoustic field, the same stepping behaviour observed by Nakamura *et al.* (1991) is apparent. For flow velocities not corresponding to these sound pressure level peaks the shedding is much less regular. The second important case has been examined by Mills *et al.* (1995). They used an applied acoustic field to control the flow past plates of different aspect ratios. They found that for particular plate aspect ratios, peaks in base suction also occurred at particular forcing frequencies. By plotting the frequencies corresponding to maximum base suctions for varying c/t they found that the same Strouhal number stepping occurred. This strongly suggests that although the mechanism of forcing is applied in a different way in each case, the same receptivity is involved.

Both external forcing and the natural response of a body to forcing (flow-induced vibrations) can result in significant modifications to the flow. For globally unstable flows, when the frequency of external forcing is gradually increased towards the natural response frequency, a bluff body (which is allowed to oscillate) exhibits (i) a resonant amplitude peak at the frequency of the imposed forcing, (ii) attenuation of the amplitude at the inherent instability frequency of the system and, (iii) a large phase shift between the motion of the body and the loading upon it (Rockwell, 1990). For rigid bodies, flow visualisation for long rectangular plates also shows that when the forcing is applied, the reattachment length of the leading-edge separated shear layer shortens and the spanwise correlation increases resulting in an increase in base suction (Stokes and Welsh, 1986; Hourigan *et al.*, 1993; Mills *et al.*, 1995). (This enhanced spanwise correlation partially justifies the two-dimensional simulations presented in this article). Sheridan *et al.* (1997) also showed that the circulation of the vortices in the wake increased significantly with forcing due to the increase in mean base suction and, in addition, the shed vortical structures were less diffuse.

The different kinds of fluid structure interaction have been classified by Naudascher and Rockwell (1994) into three categories: Extraneously induced excitation (EIE), Instability induced excitation (IIE) and Movement-induced excitation (MIE). EIE occurs when the fluctuations to the flow field and pressure are from an independent external source such as upstream turbulence, acoustic forcing (eg, Mills *et al.*, 1995) and the velocity perturbation used in this study. Instabilities that are inherent to the flow (IIE) can be further catagorised into leading edge vortex shedding (LEVS), impinging leading edge vortex shedding (ILEVS) , trailing edge vortex shedding (TEVS) and alternate edge vortex shedding (AEVS). The impinging leading edge vortex (ILEV) mode has been shown by Naudascher and Wang (1993) to be the dominant mode of vortex formation for rectangular plates between $c/t=3$-16. As the shear layer does not impinge on the trailing edge but forms discrete vortices which then interact with the trailing edge, ILEV is a better description of this instability (than the original classification of it as an impinging shear layer instability). Structures which vibrate due to fluid forces can experience MIE including phenomena such as flutter and lock-on.

This present study presents flow visualisation for both the perturbed and unperturbed cases to illustrate the mechanism underpinning the flow dynamics. First, the natural shedding case is presented and demonstrates that at low Reynolds numbers (Re=400), the leading-edge shedding exhibits the stepwise change in Strouhal number based on chord found experimentally by Nakamura *et al.* (1991) and computationally by Ozono *et al.* (1992). (Throughout this article, Reynolds number and Strouhal number are based on plate thickness unless otherwise specified.) A small oscillatory cross-flow perturbation is then applied (2.5% of free-stream velocity measured away from the plate), which can lock the shedding over a wide range of Strouhal numbers. Time-averaged base pressure measurements are taken over a wide range of St and c/t and, when compared with those observed by Mills *et al.* (1995), are found to possess similar trends. Finally, flow

visualisations show the interactions between the leading- and trailing-edge vortices when the flow is locked to the forcing and demonstrate the phasing of leading- and trailing-edge shedding.

2. Numerical Technique

The spectral element method has been used for the computations. This method can be characterised as a high-order Galerkin finite-element method with an emphasis on striking a balance between the geometrical adaptibility of (low order) *h*-type methods and the superior convergence of (high order) *p*-type schemes such as global spectral methods. The current implementation incorporates a number of techniques to increase the computational efficiency. This method has been used successfully to simulate the two and three-dimensional wake flow of a circular cylinder and predicted the two wake instability modes (*Mode A* and *Mode B* (Williamson 1988; Thompson *et al*., 1994, 1996)) for the first time.

The implementation employs the classical three-step splitting scheme for the time stepping as described in Karniadakis *et al*. (1991). Each timestep uses three substeps to treat the advection, mass conservation/pressure and diffusion terms of the Navier-Stokes equations. The Navier-Stokes equations are discretised in conservative form form which leads to discrete energy conservation. The pressure and implicit viscous substeps result in linear matrix problems. The matrices are not a function of time and so only need to be inverted once at the beginning of the calculations. Subsequently these steps only involve a (sparse) matrix multiply. The non-linear term has to be treated explicitly. Typically this is done using the third-order Adams-Bashforth scheme. The temporal derivatives from the viscous substep are treated using the Crank-Nicolson method. Higher-order boundary conditions are applied to the Poisson equation for the pressure substep which result in at least second-order overall time accuracy for the velocity field. The time-step that was used in these simulations was 0.007 dimensionless time units (scaled by the upstream velocity and plate thickness). This is at most 1/700th of a shedding period. Further details of the method can be found in Thompson *et al*. (1996), and Karniadakis and Triantafyllou (1992).

The boundary conditions applied at the boundaries of the computational domain are, (i) no slip on the plate, (ii) zero normal velocity derivative at the outflow boundary and, (iii) on the side and inflow boundary the velocity was taken as uniform in the horizontal direction plus a sinusoidally varying vertical component for the forced cases.

Figure 2 shows a typical mesh system used for the simulations. This particular one is for a chord to thickness ratio of 10. The mesh has 7 x 7 nodes per element, *i.e*. 6th order Lagrangian polynomials in each direction. The boundaries have been extended far enough to ensure good accuracy for the base pressure measurements. The inflow boundary and outflow boundaries are placed 24 and 28 plate widths from the leading and trailing edges respectively. The side boundaries are typically positioned 20 plate widths from the plate. Increasing these distances further changed base pressure measurements by less than 3% at the Reynolds number at which the simulations were carried out ($Re = 400$). Measurement of base pressure as a function of time is used to ascertain if the flow has reached an asymptotic state.

For the forced cases, the applied perturbation is a sinusoidal velocity fluctuation of 2.5% of the mean flow applied in the vertical direction on all outer boundaries except the outflow boundary.

As a further check on accuracy, simulations were performed with the mesh used for the simulations at plate aspect ratio of 10, but with 9x9 nodes per element. In this case, the Courant restriction for the convective substep required that the timestep be reduced. A timestep of 0.005 dimensionless time units was required to ensure stability. A plot of the mean base pressure as a function of frequency is shown in Figure 3. Increasing the spatial and temporal accuracy does not significantly alter the predictions; typical change is less than 1%.

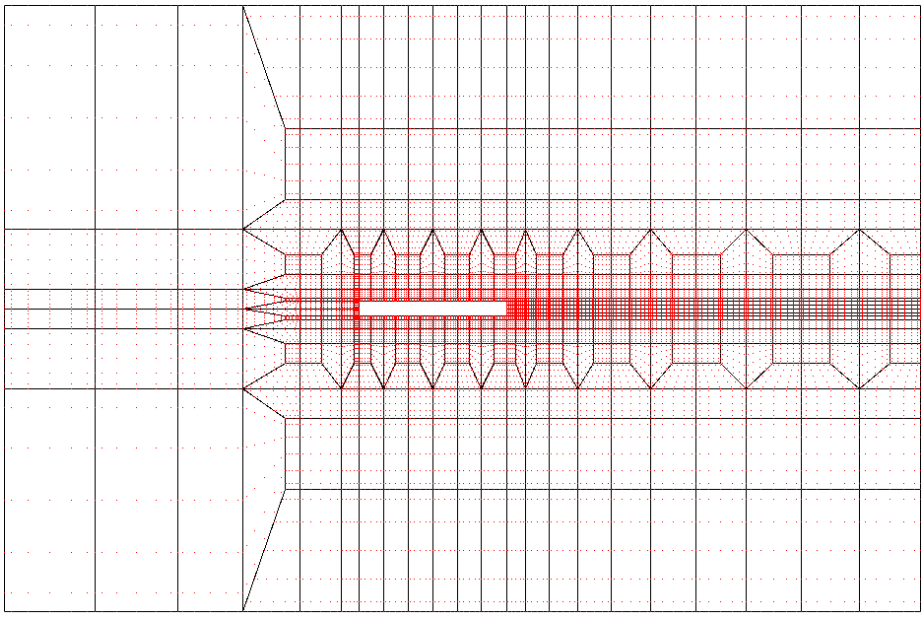


Figure 2 Typical spectral-element mesh system used for the simulations. The mesh is concentrated near the plate and extended far enough to minimise the effect of the boundaries. Sixth-order polynomial interpolation is used in each element. The nodes are shown in red.

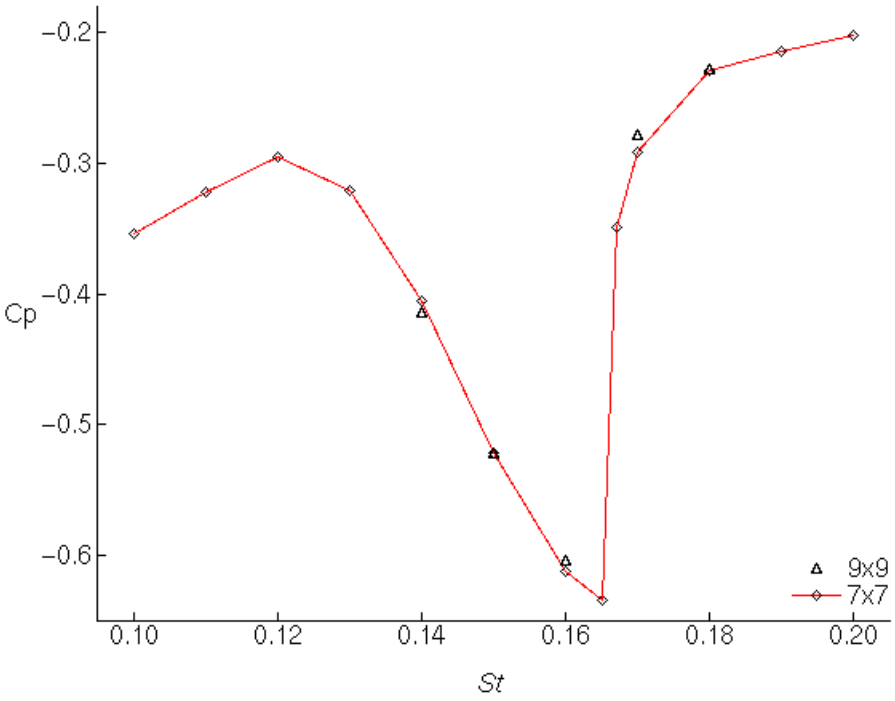


Figure 3 Comparison of Base Pressure Coefficient as a function of (applied) Strouhal number for plate aspect ratio of 10:1. The diamonds represent the results using 7x7 nodes per (macro) element, while the triangles show results for the simulations with 9x9 nodes/element.

3. Results

3.1 No Perturbation

Simulations without forcing were performed for plates with c/t between 3 and 16. For c/t less than or equal to 10, the predicted flows reached an asymptotic state with a single shedding frequency. A plot of the predicted vortex shedding Strouhal numbers, together with results of previous studies, showing the stepwise increase is shown in Figure 4. For plates with $c/t > 10$ the predicted flows did not in

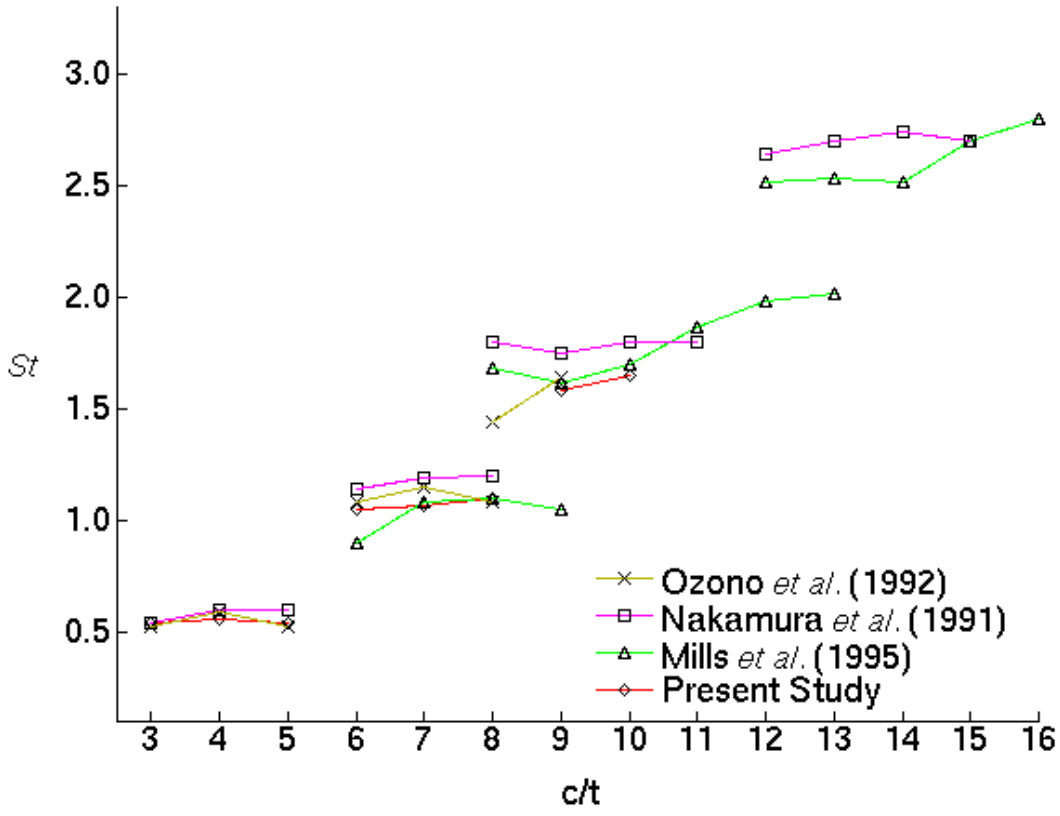


Figure 4 Plot of Strouhal number based on chord versus plate length showing the stepwise increase in *St* for the natural shedding cases together with previous published results. Data for Mills *et al*. (1995) are the Strouhal numbers of the local maxima in mean base suction.

general reach asymptotic states with a single dominant frequency; the exception was for the chord to thickness ratio c/t=13 which did attain a periodic state. The numerical integration times were in excess of 600 time units. (This integration time corresponds to over 100 shedding cycles.) It is unclear whether periodic states would be reached with longer integration times. Simulations by Ozono *et al.* (1992), and Ohya *et al.* (1992) at *Re*=1,000 showed that the flow displayed one dominant frequency between $3 < c/t < 9$ in agreement with the present simulations.

The different Strouhal number steps shown in Figure 4 represent different modes of shedding and are conjectured to result from a feedback loop. This loop consists of vortices shed from the separating and reattaching shear layer at the leading edge, traversing the chord of the plate, interacting with trailing edge and generating a pressure pulse that travels upstream to excite and control the leading-edge separating shear layer, thereby locking subsequently shed leading-edge vortices. This feedback loop is similar to that observed in other bluff body flows and was called an *impinging shear layer instability by* Rockwell and Naudascher (1978), and has more recently been designated a *type II global instability* by Rockwell (1990). In this case, the shear layer has already rolled up before reaching the trailing edge of the plate, so strictly the instability can be characterised as an *impinging vortex instability* (Mills *et al.*, 1995).

For aspect ratios for which the shedding asymptoted to a single frequency, c/t =3-5 exhibited the first mode of shedding with St_c = 0.6. This corresponded to a single leading-edge vortex convecting along the plate at any time. The feedback loop controlled the next shed vortex. The leading-edge shedding for larger aspect ratio ranges, c/t = 6-8, 9-10 and 13, represented the second, third and fourth shedding modes respectively. Hence there were (n =) two, three and four vortices above the plate for these flows (and the feedback loop controls the shedding of the second, third and fourth subsequently shed leading-edge vortex respectively.) The Strouhal number based on chord is approximately constant within each range and is given by $0.6n$. These modes of shedding are shown by in the animations of vorticity plots in Movie 1. As

observed by Ozono *et al*. (1992), the flow is more regular at the beginning of each step (i.e. c/t = 3, 6 and 9) and this deteriorates with increasing c/t until it jumps to the next step. This results in higher mean base suction and fluctuating lift forces at the begining of each step as shown in Table 1. This weakening of the vortex locking results from a competition between the natural shedding from the trailing edge and forcing from shed leading-edge vortices leading to a loss in the periodic nature of the base pressure at c/t = 5 and 8. This is consistent with the measurements of lift coefficient predicted by Ozono *et al*. (1992) and Ohya *et al*. (1992). Figure 5 show a trace of the base pressure at c/t = 7, 8 and 9 where the shedding changes mode.

c/t	St_t	Mean C_p	Mean C_D	σ_{Cl}
3	0.180	-0.669	0.725	0.558
4	0.140	-0.422	0.601	0.544
5	0.108	-0.310	0.561	0.544
6	0.175	-0.631	0.722	0.673
7	0.153	-0.495	0.657	0.601
8	0.138	-0.334	0.577	0.535
9	0.175	-0.547	0.684	0.709
10	0.165	-0.481	0.644	0.666
13	0.167	-0.475	0.658	0.742

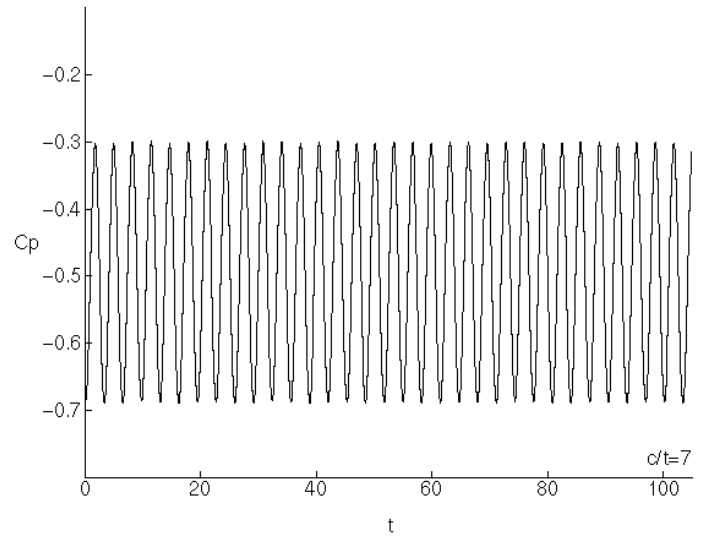
Table 1: Variation of the drag and fluctuating lift experienced by the plate showing the increase in both force components when the plate aspect ratio is a multiple of 3.

3.2 With Perturbation Applied

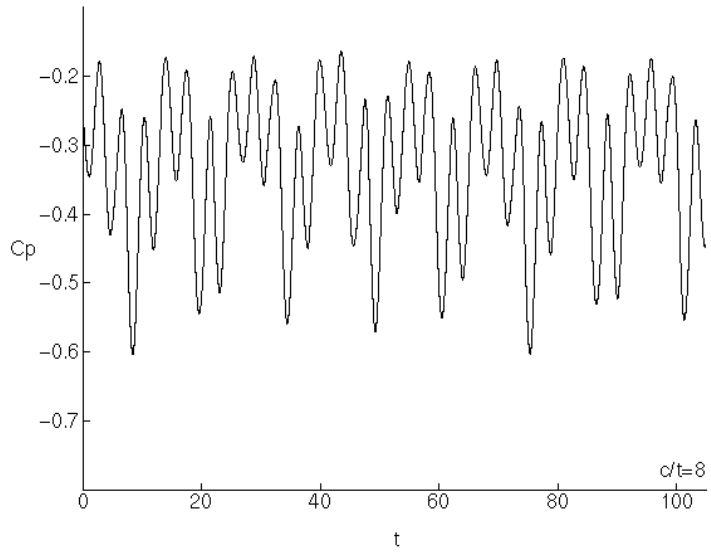
A small sinusoidal perturbation with amplitude of 2.5% of free-stream velocity is applied at the free-stream boundaries to lock the flow. Although many studies employ an acoustic field to control flows, often little attention is paid to the detailed specification of the field. As a result, it can be difficult to replicate such experiments and analyse the interaction between the acoustic and flow fields. Movie 2 shows a snapshot of the perturbation velocity field (in the absence of any free-stream velocity) at St = 0.17 and c/t = 10. The perturbing flow does accelerate around the edges of the plate (as does the mean flow) but still remains small relative to the upstream flow, whose magnitude is shown by the blue vector in Movie 2. Although relatively small, this magnitude of perturbation is enough to lock the flow over a wide range of Strouhal numbers, typically between St=0.08 to St=0.25 for the plates used which had c/t values in the range 6 - 16. The 2.5% background forcing is equivalent to approximately a 5% perturbation in the neighbourhood of the leading and trailing edges. This level is close to the effective acoustic forcing amplitude in the vicinity of the edges applied in the experiments of Mills *et al.* (1995).

Simulations were performed for a wide range of St for c/t = 6-16 and the time mean base pressure coefficient Cp was predicted. (This was calculated by determining the time mean of the pressure coefficient at the midpoint of the trailing edge.) These predictions together with the measurements of Mills *et al*. (1995) are presented in Figure 6; it can be seen that although the flow is locked on over a wide range of forcing frequencies, it is most receptive (as indicated by local maxima in base suction) at one, or at most two, frequencies for each c/t.

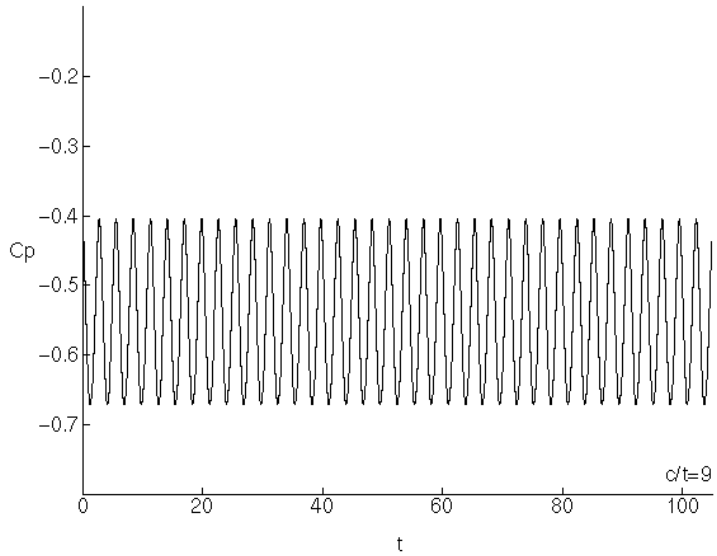
This receptivity is clarified by considering the base suction response for each particular aspect ratio as the forcing frequency is varied. Beginning with c/t = 6, a local maximum base suction is reached for St = 0.17. As c/t is increased to 7, the Strouhal number at which maximum base suction occurs drops to St = 0.16, then St = 0.14 at c/t=8 and St = 0.12 for c/t = 9. While the local base suction maximum is shifting to lower Strouhal numbers, another local peak emerges at St = 0.174 for c/t = 8. Then with increasing c/t, this peak shifts to St = 0.162 at c/t = 9, St =0.165 at c/t = 10, St = 0.155 at c/t = 11, St = 0.14 at c/t = 12 and St = 0.13 for c/t = 13. This pattern repeats with another local peak developing at St = 0.157 for c/t = 13 which moves



(a)



(b)



(c)

Figure 5 A 100 time unit sample of the base pressure coefficient of the natural shedding case at (a) *c/t*=7, (b) *c/t*=8 and (c) *c/t*=9 taken after the shedding has reached an asymptotic state.

to $St = 0.155$ at $c/t = 14$, $St = 0.155$ at $c/t = 15$ and $St = 0.145$ at $c/t = 16$. A similar trend is also evident in experimental mean base suction measurements by Mills *et al*. (1995) plotted alongside in Figure 6.

The predicted and observed mean pressure measurements show some differences presumably due to modelling assumptions. The experimental results were performed at approximately $Re = 9{,}000$ with an acoustic field used to lock the flow. The numerical simulations were carried out for $Re = 400$ and were restricted to two dimensions, which resulted in the vortices remaining more coherent along the plate surface (as opposed to the formation of hairpin structures in the observations) and exerting a larger influence at the trailing edge; consequently, the magnitude of the predicted base pressure is higher than the observation. Nevertheless, the predicted and observed flows show a distinct staging in the mean base suction with c/t and this will be the focus of further discussion.

To assist in comparing the flow states leading to different base pressure suctions, vorticity plots are presented for the cases where there are local maxima in base pressure. Figure 7 are plots taken at 90° into the sinusoidal forcing cycle when the perturbation is at its maximum in the upward direction. It can be seen that the peaks in base suction occur when the flow is locked into distinct shedding modes. For $c/t = 6$-9, $c/t = 8$-13 and c/t=13-16, the flow is locked into the $n = 2$, $n = 3$ and $n = 4$ modes respectively which correspond to the number of vortices on the side face. Also note that the leading edge and trailing edge are in the same phase of their shedding cycle suggesting that the phase of shedding influences the base pressure. At $c/t = 8$, 9 and 13, there are two local maxima in base suction which Figure 7 illustrates to correspond to two different shedding modes; for the higher mode shedding at the trailing edge is 180° out of phase relative to the lower mode. These plate aspect ratios in the transition region between shedding modes.

It is not surprising then that Figure 8, a plot of the Strouhal number based on chord corresponding to a local maximum in base suction as a function of c/t, shows a stepwise increase. There is good agreement between the predicted Strouhal numbers and the results of Mills *et al*. (1995) for the lower aspect ratios but the predicted values of the Strouhal numbers differ slightly more for the higher shedding modes (*i.e*., $n = 3$ and $n = 4$). In addition, in the experiments, the Strouhal number (based on thickness) for which the maximal base suction occurs tends to increase with mode number, while for the simulations show the opposite behaviour as shown in Table 2 below. A possible explanation for this is that the convection speed of the vortices may not follow the same trend in the two cases, as a result of different Reynolds number and three-dimensional effects. In the experiments of Nakamura *et al*. (1991) the trend of increasing Strouhal number for the higher modes was also observed while the two-dimensional unforced simulations of Ozono et al. (1992) and Ohya et al. (1992) showed the opposite behaviour in agreement with the current simulations. To help resolve this issue a program of three-dimensional simulations is currently being undertaken.

c/t	**St (numerical)**	**St (experimental)**
6	0.170	0.15
10	0.165	0.17
14	0.155	0.195

Table 2: Variation of natural Strouhal number (based on the shedding frequency) as a function of plate aspect ratio c/t. The experimental results of Mills *et al*. (1995) are compared with those obtained from the simulations.

Ozono *et al*. (1992) observed in the case of flow around rectangular plates in the absence of external forcing that, at the start of each step, the flow is more strongly locked. A similar result is observed in the current predictions. With increasing c/t, it is found that there is less regularity in the vortex shedding until it eventually locks on to the frequency of the next step in Strouhal number based on chord. It can also be

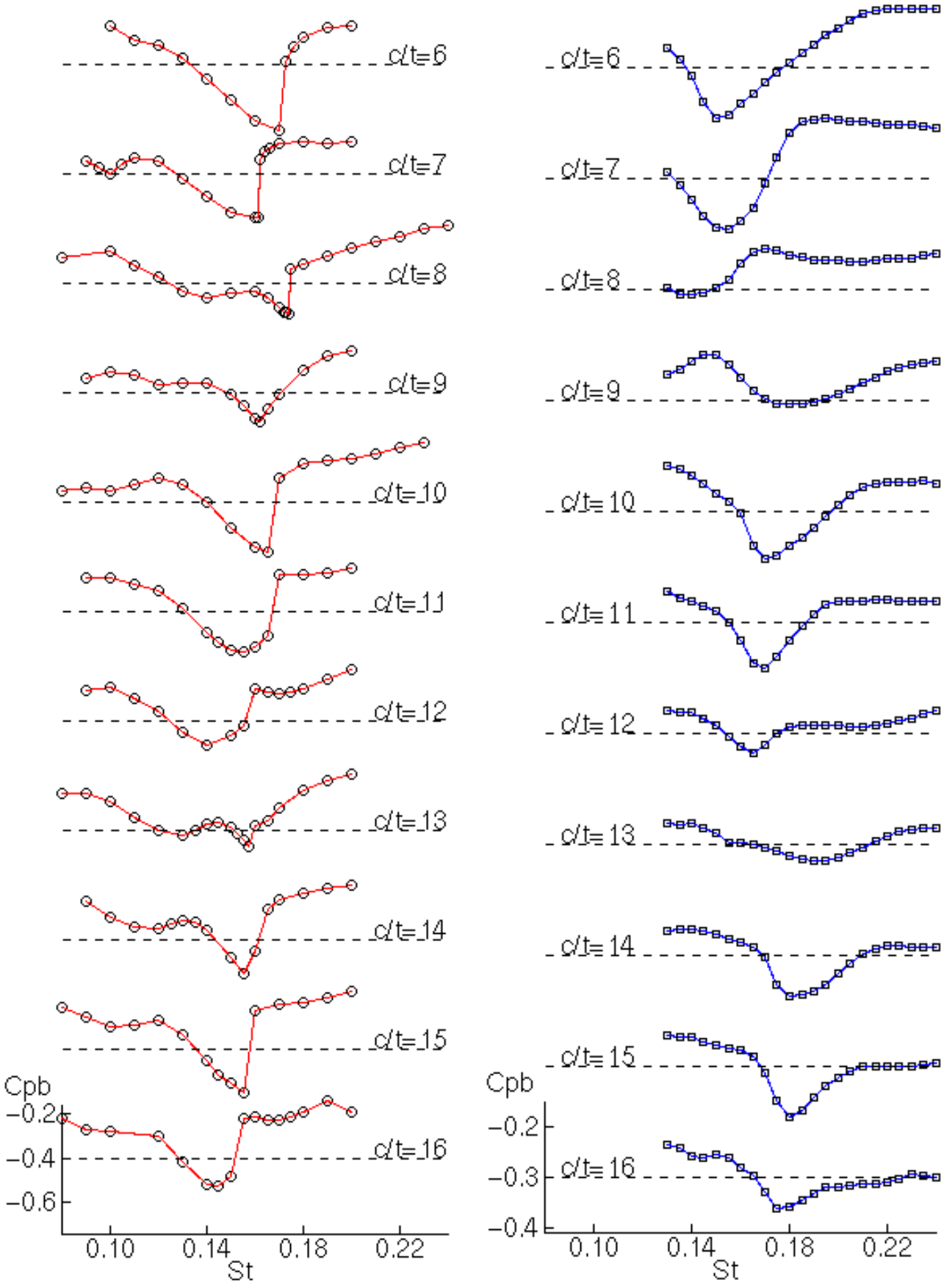


Figure 6 Base pressures as a function of perturbation frequency. ○ - predicted results from the current simulations; □ - are measured values from Mills *et al*. (1995). The dotted lines indicate reference levels: -0.4 for the simulations (left), and -0.3 for the experimental results (right).

observed that, in those cases with forcing, at the beginning of each step, (*i.e.*, c/t = 6, 10 and 14), the magnitude of base pressure is larger and decreases with increasing c/t until the flow state jumps to the next mode. This is evident in both the numerical results and the experimental results of Mills *et al.* (1995) both shown by Figure 6. If one considers the plots of vorticity in Figure 7, the vortex forming at the trailing edge of the plate appears strong at the beginning of each stage resulting in the larger pressure drop. As seen in Figure 7, the phase of shedding from the trailing edge matches at the peak base suction for varying c/t, this suggests that the trailing edge shedding is more receptive to the flow perturbations at the beginning of each step where the frequency is higher and with increasing c/t, it is less receptive to the lower frequency until jumping to the next mode.

Movie 3 contains a selection of sequential images showing the effects of the perturbation to the flow. Generally, the forcing causes the leading edge vortices to roll up tighter than the unperturbed flow. This has been observed by Sheridan *et al.* (1997). Movie 3a shows the flow at c/t = 10 with an external forcing at St = 0.12. At this relatively low forcing frequency, the trailing edge shedding is present but the vortices are relatively weak and the formation length is large. Also the leading and trailing edge vortices do not merge in the wake. This results in a weaker base suction. Movie3b represents the flow for a perturbation frequency of St = 0.165. This simulation has a strong trailing-edge shedding with a short formation length and the leading and trailing edge vortices merge in the wake. This results in a strong base suction. Movie 3c is for a perturbation frequency of St = 0.174 and c/t = 8. This result is similar to the previous except that it is shedding 180° out of phase relative to the previous simulation. This is common for the cases which result in local peaks in base suction at higher forcing frequencies (*i.e.*, c/t = 8, 9 and 13). Movie 3d is for a perturbation frequency of St = 0.20 and c/t = 10. At the higher frequencies, trailing-edge shedding is suppressed and this results in a lower base suction. The shedding from the trailing edge is a result of the roll up of the boundary layer between vortices from the leading edge. At high frequencies, the leading-edge vortices are closer together and this restricts the amount circulation in the boundary layer resulting in a suppressed shedding from the trailing edge. The trailing-edge shedding is a strong absolute instability, presumably naturally unstable only over a narrow frequency range. At higher forcing frequencies the trailing edge shedding is not receptive to the external forcing. In addition, interference from leading-edge vortices as they pass the trailing-edge seems to cause trailing-edge shedding to be suppressed altogether.

The staging of the peaks in base pressure is similar to the natural shedding case shown earlier. The numerical model does not show the experimentally observed trend of increasing St at the start of each stage. However, both results presented here and those of Mills *et al.* (1995) show that the peak base suction is stronger at the shorter plate lengths for each step. Since large base suctions are associated with strong and tight vortex shedding from the trailing edge, this result probably indicates that the natural frequency for trailing-edge shedding is closer to the applied forcing frequency at the start of each step and as the natural and applied frequencies become different the response is less strong.

4. Conclusions

Extensive simulations of the *two-dimensional* flow around long plates of rectangular cross-section, both with and without transverse forcing, have been carried out. The Reynolds number was chosen to be 400 (so that good resolution of the flow could be achieved). This was sufficiently high to produce strong shedding from both the leading and trailing edges; however, it is believed that the results from the simulations are generally applicable to significantly higher Reynolds numbers. This is consistent with previous numerical simulations for the unforced case at Re = 1000 (Ozono *et al.*, 1992 and Ohya *et al.*, 1992), and experimental results for the forced cases at Reynolds numbers of order 10^4 (Mills *et al.*, 1995).

The flow without perturbation locks on to integer modes of shedding at Re = 400 resulting in a stepwise increase in Strouhal number (based on chord) with increasing aspect ratio. Under a sinusoidal velocity perturbation, measurements of base pressure reveal that the most receptive cases (i.e local maxima in base suction) also correspond to integer modes of shedding. This results in the stepwise increase in Strouhal number based on chord for local maxima in mean base suction for increasing c/t. Mean base pressure is dependent on the trailing edge shedding. Both the base suction and magnitude of the fluctuating lift are greater at the beginning of each step and decrease until the flow switches to the next integer shedding mode

at the beginning of the next Strouhal number step. This behaviour appears to be due to the narrow range of frequencies at which the trailing edge is receptive.

Although the two-dimensional simulations at low Reynolds number appear to capture many of the essential features of the flow as observed in the experiments, the real flow is three-dimensional even at these low Reynolds numbers. Details such as the actual values of the base suctions and the behaviour of the most receptive Strouhal number as a function of the plate aspect ratio (Table 2) cannot be extracted from the current simulations. At present, three-dimensional simulations are being performed to examine some of these unresolved aspects. The results of those simulations will be reported elsewhere.

Acknowledgements

The support of an Australian Research Council grant is acknowledged. Tan Boon Thong acknowledges the support of a Monash Postgraduate Award. The authors thank John Sheridan and Richard Mills for helpful discussions.

References

Bearman, P.W. (1984) Vortex Shedding from Oscillating Bluff Bodies, *Annual Review of Fluid Mechanics*, **16,** 195-222.

Bearman, P.W. and Obasaju, E.D. (1982) An Experimental Study of Pressure Fluctuations on Fixed and Oscillating Square-Sectioned Cylinders, *Journal of Fluid Mechanics*, **119**, 297-321.

Bearman, P.W. and Trueman, D.M. (1972) An Investigation of the Flow around Rectangular Cylinders, *Aeronautical Quarterly*, 229-237.

Hourigan, K., Mills, R., Thompson, M.C., Sheridan, J., Dilin, P. and Welsh, M.C. (1993) Base Pressure Coefficients for Flows around Rectangular Plates, *Journal of Wind Engineering*, **49**, 311-318.

Karniadakis, G.E., Israeli, M. and Orszag, S.A. (1991) High-Order Splitting Methods for the Incompressible Navier-Stokes Equations, *Journal of Computational Physics*, **97**, 414-443.

Karniadakis, G.E. and Triantafyllou, G.S. (1992) Three-dimensional Dynamics and Transition to Turbulence in the Wake of Bluff Objects, *Journal of Fluid Mechanics*, **238**, 1-30.

Koch, W. (1985) Local Instability Characteristics and Frequency Determination of Self-Excited Wake Flows, *Journal of Sound and Vibrations*, **99**, 53-83.

Mills, R., Sheridan, J., Hourigan, K. and Welsh, M.C. (1995) The Mechanism Controlling Vortex Shedding from Rectangular Bluff Bodies, *Proceedings of the Twelfth Australasian Fluid Mechanics Conference*, December, Sydney, Australia, 227-230.

Nakamura, Y., Ohya, Y. and Tsuruta, H. (1991) Experiments on the Vortex Shedding from Flat Plates with Square Leading Edge and Trailing Edges, *Journal of Fluid Mechanics,* **15**, 1025-1036.

Nakayama, R., Nakamura, Y., Ohya, Y. and Ozono, S. (1993) A Numerical Study on the flow around flat plates at low Reynolds Numbers, *Journal of Wind Engineering and Industrial Aerodynamics,* **46&47,** 255-264.

Naudascher, E. and Rockwell, D. (1994) Flow-Induced Vibration - An Engineering Guide, *Rotterdam, Editor: A. Balkema*.

Naudascher, E. and Wang, Y. (1993) Flow-Induced Vibration of Prismatic Bodies and Grids of Prisms, *Journal of Fluid and Structures,* **7**, 341-373.

Ohya, Y., Nakamura, Y, Ozono, S., Tsuruta, H. and Nakayama, R. (1992) A Numerical Study of Vortex Shedding from Flat Plates with Square Leading and Trailing Edges, *Journal of Fluid Mechanics*, **236**, 445-460.

Okajima, A., Nagahisa, T. and Rokugoh, A. (1990) A Numerical Analysis of Flow around a Rectangular Cylinder, *JSME International Journal II,* **33:4**, 702-711.

Okajima, A., Ueno, H. and Sakai, H. (1992) Numerical Simulations of Laminar and Turbulent Flows around a Rectangular Cylinder, *International Journal for Numerical Methods in Fluids,* **15**, 999-1012.

Ozono, S., Ohya, Y., Nakamura, Y. and Nakayama, R. (1992) Stepwise Increase in the Strouhal Number for Flows around Flat Plates, *International Journal for Numerical Methods in Fluids,* **15**, 1025-1036.

Parker, R. (1997) Aeroacoustics, *International Journal of Fluid Dynamics (WWW), **1**, Article 1*.

Rockwell, D. (1990) Active Control of Globally-Unstable Separated Flows, Proceedings of the ASME Symposium on Unsteady Flows, Toronto, 1990.

Rockwell, D. and Naudascher, E. (1979) Self-Sustained Oscillations of Impinging Free Shear Layers, *Annual Review of Fluid Mechanics,* **11**, 67-94.

Roshko, A. (1961) Experiments of Flow Past a Circular Cylinder at Very High Reynolds Number, *Journal Fluid Mechanics*, **10**, 345-356.

Sheridan, J., Hourigan, K. and Mills, R. (1997) Vortex Structures in Flow over a Rectangular Plate, *Transactions of the ASME*, Paper AD-Vol 53-1 (November), 85-91.

Soria, J. and Wu, J. (1992) The Characteristic of the Instability of the Separated Shear Layer from a Square Leading Edge Flat Plate, *Proceedings of the Eleventh Australasian Fluid Mechanics Conference*, December, Hobart, Australia, 391-394.

Stokes, A.N. and Welsh, M.C. (1986) Flow-Resonant Sound Interaction in a Duct Containing a Plate II: Square Leading Edge, *Journal of Sound and Vibration,* **104**, 55-73.

Thompson, M.C., Hourigan, K. and Sheridan, J. (1994) Three-Dimensional Instabilities in the Wake of a Circular Cylinder, *Proceedings of the International Colloquium on Jets, Wakes and Shear Layers*, April 1994, CSIRO Division of Building, Construction and Engineering, Melbourne, Australia, *10.1 - 10.9*.

Thompson, M.C., Hourigan, K. and Sheridan, J. (1996) Three-Dimensional Instabilities in the Wake of a Circular Cylinder, *International Journal of Experimental Heat Transfer, Thermodynamics, and Fluid Mechanics,* **12**, 190-196.

Williamson, C.H.K. (1988) Defining a Universal and Continuous Strouhal-Reynolds Number Relationship for the Laminar Vortex Shedding of a Circular Cylinder, *Physics of Fluids,* **31**, 2742.